Title	Solvent-Dependent Conformation of Amylose Tris(Phenylcarbamate) as Deduced from Scattering and Viscosity Data
Author(s)	Fujii, Taichi; Terao, Ken; Tsuda, Maiko et al.
Citation	Biopolymers. 2009, 91(9), p. 729-736
Version Type	AM
URL	https://hdl.handle.net/11094/53323
rights	
Note	

Solvent-Dependent Conformation of Amylose Tris(Phenylcarbamate) as Deduced from Scattering and Viscosity Data

Taichi Fujii,[1] Ken Terao,[1] Maiko Tsuda,[1] Shinichi Kitamura,[2] Takashi Norisuye[1]

[1]*Department of Macromolecular Science, Osaka University, 1-1, Machikaneyama-cho, Toyonaka, Osaka, 560-0043, Japan*

[2]*Graduate School of Life and Environmental Sciences, Osaka Prefecture University, Gakuen-cho, Nakaku, Sakai, Osaka 599-8531, Japan*

Correspondence to K. Terao: (E-mail: kterao@chem.sci.osaka-u.ac.jp)

ABSTRACT: The z-average mean-square radius of gyration $<S^2>_z$, the particle scattering function $P(k)$, the second virial coefficient, and the intrinsic viscosity $[\eta]$ have been determined for amylose tris(phenylcarbamate) (ATPC) in methyl acetate (MEA) at 25 °C, in ethyl acetate (EA) at 33 °C, and in 4-methyl-2-pentanone (MIBK) at 25 °C by light and small-angle X-ray scattering and viscometry as functions of the weight-average molecular weight in a range from 2×10^4 to 3×10^6. The first two solvents attain the theta state, while the last one is a good solvent for the amylose derivative. Analysis of the $<S^2>_z$, $P(k)$, and $[\eta]$ data based on the wormlike chain yields h (the contour length or helix pitch per repeating unit) = 0.37 ± 0.02 and λ^{-1} (the Kuhn segment length) = 15 ± 2 nm in MEA, $h = 0.39 \pm 0.02$ and $\lambda^{-1} = 17 \pm 2$ nm in EA, and $h = 0.42 \pm 0.02$ nm and $\lambda^{-1} = 24 \pm 2$ nm in MIBK. These h values, comparable to the helix pitches ($0.37 - 0.40$ nm) per residue of amylose triesters in the crystalline state, are somewhat larger than the previously determined h of 0.33 ± 0.02 nm for ATPC in 1,4-dioxane and 2-ethoxyethanol, in which intramolecular hydrogen bonds are formed between the C=O and NH groups of the neighbor repeating units. The slightly extended helices of ATPC in the ketone and ester solvents are most likely due to the replacement of those hydrogen bonds by intermolecular hydrogen bonds between the NH groups of the polymer and the carbonyl groups of the solvent.

Keywords: amylose; wormlike chain; light scattering; SAXS; viscosity

INTRODUCTION

Amylose tris(phenylcarbamate) (ATPC), whose chemical structure is shown in Chart 1, behaves as a semiflexible chain[1-7] with locally helical structure[8,9] in dilute solution.   Its stiffness expressed in terms of the Kuhn segment length λ^{-1} (about 20 nm) in the wormlike chain model[10] or more generally the stiffness parameter in the helical wormlike chain[11] is much higher than that of amylose (4 nm).[12,13]   Very recently,[9] we analyzed the scattering function and viscosity data for the amylose derivative based on the wormlike chain model, and found that the helix pitch h per residue or the contour length per residue of ATPC is 0.33 ± 0.02 nm in 1,4-dioxane (DIOX) and 2-ethoxyethanol (2EE), i.e., a value appreciably smaller than what is known for the helices of amylose triesters (0.37 – 0.40 nm) in the crystalline state.[14,15]   We explained this shorter pitch as due to the intramolecular hydrogen bonding between C=O and NH groups of neighbor repeating units of ATPC on the basis of the observed IR (infrared absorption) spectra in the two solvents.
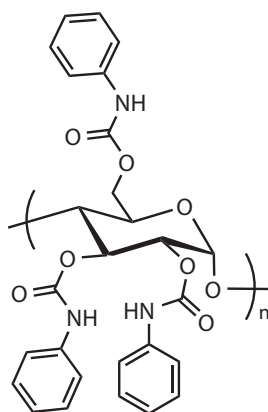

CHART 1   Chemical structure of amylose tris(phenylcarbamate) ATPC.

The above work prompted us to see whether the shorter helix pitch is characteristic of ATPC in solution or extends to a value comparable to 0.37 – 0.40 nm for the crystalline amylose triesters when the solvent conditions are changed.   Except for our data in DIOX and 2EE, virtually no information on h was available for this polymer in the literature.   In this situation, we deemed it legitimate to use as solvents ketones or esters whose C=O groups are capable of strongly interacting with the NH groups of ATPC, even though such solvents did not always allow IR spectroscopy in a relevant range of wavelength.

The present study was undertaken to determine h and λ^{-1} for ATPC in methyl acetate (MEA), ethyl acetate (EA), and 4-methyl-2-pentanone (MIBK) by light and small-angle X-ray scattering (SAXS) and viscometry.   The two ester solvents were found to attain the theta state (see the Experimental section).   We also found that, as shown in Figure 1, the intrinsic viscosity $[\eta]$ of an ATPC sample (ATPC3M)[9] with a weight-average molecular weight M_w of 3.27×10^6 (at 25 °C) depends significantly on the molar volume v_M of the solvent while that of cellulose tris(phenylcarbamate) (CTPC) sample[16] with a comparable M_w of 2.62×10^6 has no such tendency.   This suggests that

the dimensions of the ATPC molecule and hence the degree of chain extension have something to do with the bulkiness around the carbonyl groups of the solvent molecules.　Since the chain extension (in the unperturbed state) arises from an increase in either h or λ^{-1} or increases in both, separate estimation of the two molecular parameters and comparison with those in DIOX and 2EE should serve to clarify solvent effects on the conformation of ATPC.
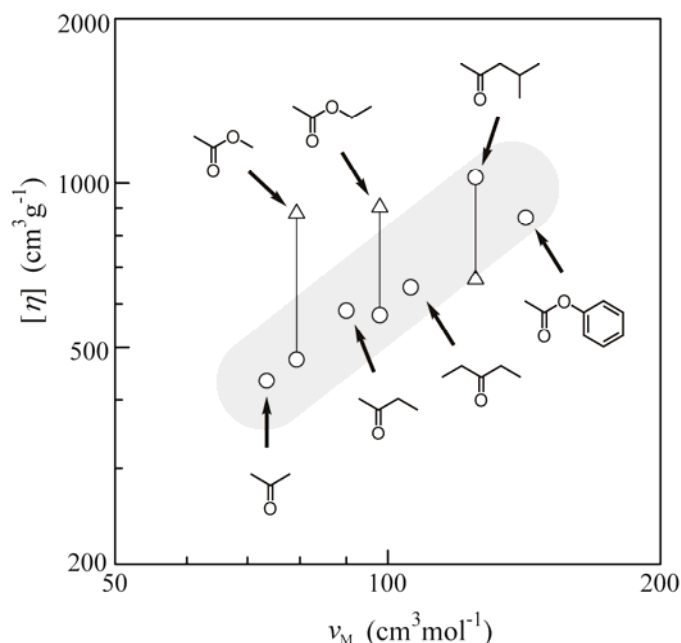

FIGURE 1　Dependence of $[\eta]$ on the molar volume of solvent for ATPC3M (circles) and a CTPC sample with $M_w = 2.62 \times 10^6$ (triangles) at 25 °C.

EXPERIMENTAL

Samples

Seven previously investigated ATPC samples[9] (ATPC3M, ATPC800K, ATPC500K, ATPC300K, ATPC200K, ATPC50K, and ATPC20K) ranging in M_w from 2×10^4 to 3×10^6 were used for the present study.　These samples with the full degree of substitution had been prepared from enzymatically synthesized amylose[17] and phenylisocyanate.　The ratios of M_w to the number-average molecular weight or those of the z-average molecular weight to M_w were in the range between 1.05 and 1.11.[9]　MEA, EA, and MIBK were purified by fractional distillation over CaH$_2$.

Light Scattering

Intensities of light scattered from ATPC solutions were measured for five higher molecular weight samples in EA, MEA, and MIBK on a Fica-50 light scattering photometer at a wavelength λ_0 of 436 nm; sample ATPC800K could not be studied in EA and MIBK because of its poor solubility in the two solvents.　The procedures including the calibration of the photometer were the same as those

described previously.[9]   The square-root plot[18] was used to evaluate M_w, the particle scattering function $P(k)$ (k denotes the magnitude of the scattering vector), the z-average mean-square radius of gyration $<S^2>_z$, and the second virial coefficient A_2.   The specific refractive index increments $\partial n/\partial c$ at $\lambda_0 = 436$, 546, and 633 nm were determined for sample ATPC800K in MEA at 20, 30, and 40 °C, for ATPC3M in EA at 10, 20, and 25 °C, and for ATPC3M in MIBK at 25 °C (see Supplementary Material for the numerical data).

In our preliminary intensity measurements, the temperature T was varied in the range between 25 and 50 °C in expectation of the presence of the theta condition near room temperature, because ATPC solutions of the three solvents became clouded at elevated temperatures, indicating that they have lower critical solution temperatures (LCST).   Figure 2 shows that A_2 for ATPC vanishes in EA at 33 °C and in MEA (within experimental errors) at any T between 25 and 40 °C.   Thus, these temperatures can be regarded as the theta points for the polymer in the respective solvents.   For MEA solutions, we chose scattering data at 25 °C (the lowest T) as those at the theta temperature; the solutions were less stable at 45 °C and higher temperatures (due to pronounced scattering-intensity fluctuation).   The A_2 values of about 1.8×10^{-4} mol cm^3 g^{-2} in MIBK, shown by the half-filled symbols in the figure, are comparable to those in DIOX, indicating that, as is the case with DIOX, MIBK at 25 °C is a good solvent for ATPC.
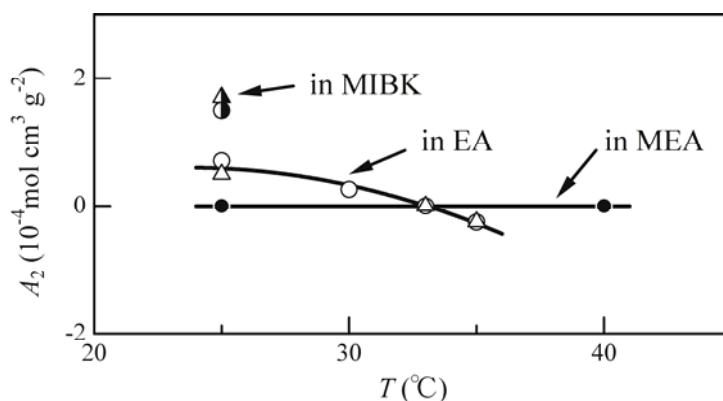

FIGURE 2   Temperature dependence of A_2 for samples ATPC3M (circles) and ATPC500K (triangles) in MEA (filled symbols), in EA (unfilled symbols), and in MIBK (half-filled symbols).

Small-Angle X-Ray Scattering

SAXS measurements were made on two samples ATPC50K and ATPC20K in MEA at 25 °C, in EA at 33 °C, and in MIBK at 25 °C with an imaging plate detector at the BL40B2 beamline in SPring-8. The camera length and λ_0 were set to be 1500 mm and 0.1 nm, respectively (see ref 9 for other experimental details).   Four solutions of different polymer mass concentrations c were studied for each combination of sample and solvent, and intensity data were extrapolated to infinite dilution using the square-root plot[18] to determine $<S^2>_z$ and $P(k)$.

Viscometry

Intrinsic viscosities at zero shear rate were determined for ATPC samples in the three solvents at the same temperatures as those in the SAXS experiment using a four-bulb low-shear capillary viscometer and conventional capillary viscometers of the Ubbelohde type; shear-rate effects on $[\eta]$ were appreciable (2%) only for the highest molecular weight sample ATPC3M in MIBK. Huggins' constants were in a range between 0.34 and 0.82, but those for ATPC20K (the lowest M_w sample) in MEA and MIBK slightly exceeded unity.

RESULTS

Figure 3 illustrates plots of $(Kc/R_0)^{1/2}$ vs c for ATPC samples in MEA at 25 °C, EA at 33 °C, and MIBK at 25 °C, where K and R_0 denote the optical constant and the reduced scattering intensity at zero scattering angle, respectively. While the indicated lines in panel (c) have positive slopes as expected for a good solvent, those in panels (a) and (b) are almost horizontal, confirming that MEA at 25 °C and EA at 33 °C are theta solvents for ATPC. The values of M_w evaluated from the intercepts for each sample in the three solvents agreed with our previous M_w in DIOX and 2EE within $\pm$ 6%. Thus, the averages of M_w's from these five solvents are presented in Table 1. The angular dependence of $P(k)^{-1/2}$ is depicted for the seven samples in the three solvents in Figure 4. The values of $<S^2>_z$ evaluated from the initial slopes (the dashed lines) are summarized in Table 1, along with those of $[\eta]$.
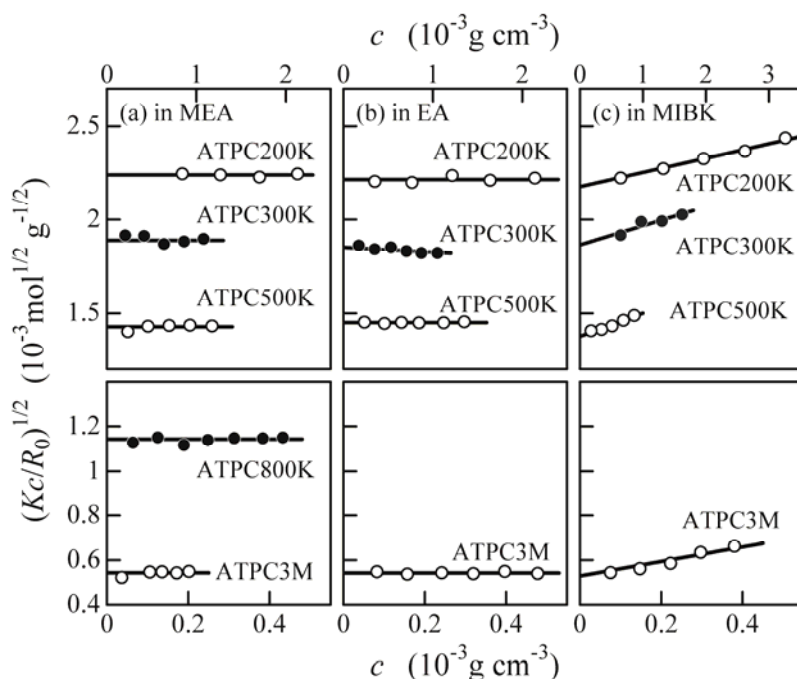

FIGURE 3 Concentration dependence of $(Kc/R_0)^{1/2}$ for indicated ATPC samples in MEA at 25 °C (a), in EA at 33 °C (b), and in MIBK at 25 °C (c).

Table 1. Numerical Results from Light Scattering, SAXS, and Viscosity Measurements on ATPC Samples in Methyl Acetate (MEA) at 25 °C, Ethyl Acetate (EA) at 33 °C, and 4-Methyl-2-pentanone (MIBK) at 25 °C

Sample	$\dfrac{M_w}{10^4}$	in MEA		in EA		in MIBK	
		$\langle S^2 \rangle_z^{1/2}$ (nm)	$[\eta]$ (cm³g⁻¹)	$\langle S^2 \rangle_z^{1/2}$ (nm)	$[\eta]$ (cm³g⁻¹)	$\langle S^2 \rangle_z^{1/2}$ (nm)	$[\eta]$ (cm³g⁻¹)
ATPC3M	333 [c]	80 [a]	475	91 [a]	495	107 [a]	1030
ATPC800K	76.5 [c]	36.1 [a]	151				
ATPC500K	49.1 [c]	30.8 [a]	126	32.9 [a]	156	39.6 [a]	226
ATPC300K	28.2 [c]	22.9 [a]	88.7	25.5 [a]	110	30.8 [a]	157
ATPC200K	19.9 [c]	18.8 [a]	62.5	21.3 [a]	67.7	24.1 [a]	88.8
ATPC50K	5.48 [d]	7.6 [b]	24.0	8.6 [b]	27.7	10.3 [b]	30.9
ATPC20K	1.87 [d]	3.5 [b]	8.7	3.8 [b]	9.8	4.0 [b]	10.6

[a] Light scattering. [b] SAXS. [c] Average of M_w's determined from light scattering in different solvents (see text). [d] Ref. 9

Figure 5(a) illustrates the molecular weight dependence of $\langle S^2 \rangle_z/M_w$ in MEA at 25 °C, EA at 33 °C, and MIBK at 25 °C along with our previous data.[9]   As M_w increases, $\langle S^2 \rangle_z/M_w$ in any solvent rises and then almost levels off at a constant.   This behavior is typical of the unperturbed wormlike chain,[19] and, as was previously found to be the case in DIOX and 2EE, excluded-volume effects on $\langle S^2 \rangle_z$ in MIBK must be small, if any.   Although the values of $\langle S^2 \rangle_z/M_w$ for low molecular weight samples in MEA, EA, and MIBK are different from one another, they are slightly larger than those in DIOX and 2EE.   This suggests that h should be somewhat larger in the former group of solvents than in the latter group, since $\langle S^2 \rangle_z$ at low M_w is sensitive not to the chain stiffness but to h.

The molecular weight dependence of $[\eta]/M_w^{1/2}$ is shown in Figure 5(b).   Interestingly, $[\eta]/M_w^{1/2}$ at low M_w is almost independent of the kind of solvent, differing from the solvent-dependent $\langle S^2 \rangle_z/M_w$ observed above.   This seemingly contrasted finding may be reconciled if an ATPC chain with a larger h (i.e., a more extended helix) has a thinner diameter.
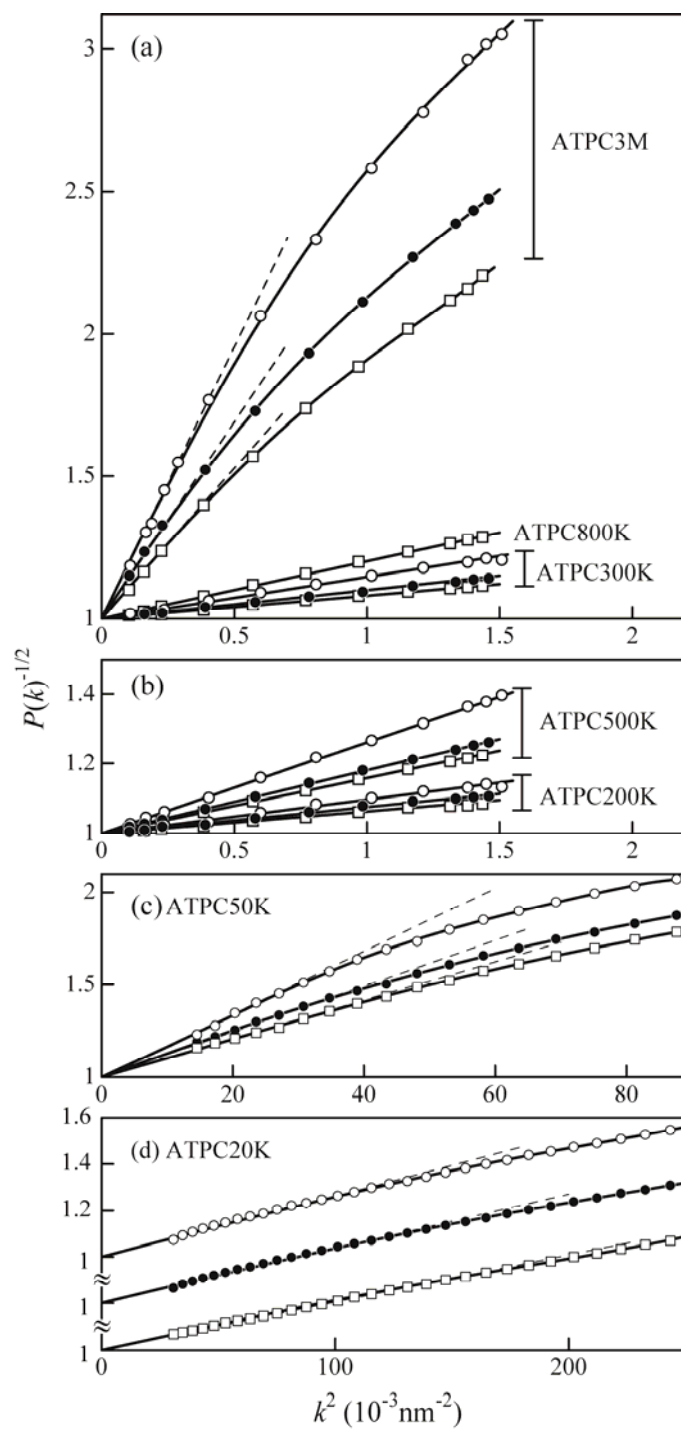
FIGURE 4   Angular dependence of $P(k)^{-1/2}$ for ATPC samples in MEA at 25 °C (squares), in EA at 33 °C (filled circles), and in MIBK at 25 °C (unfilled circles).
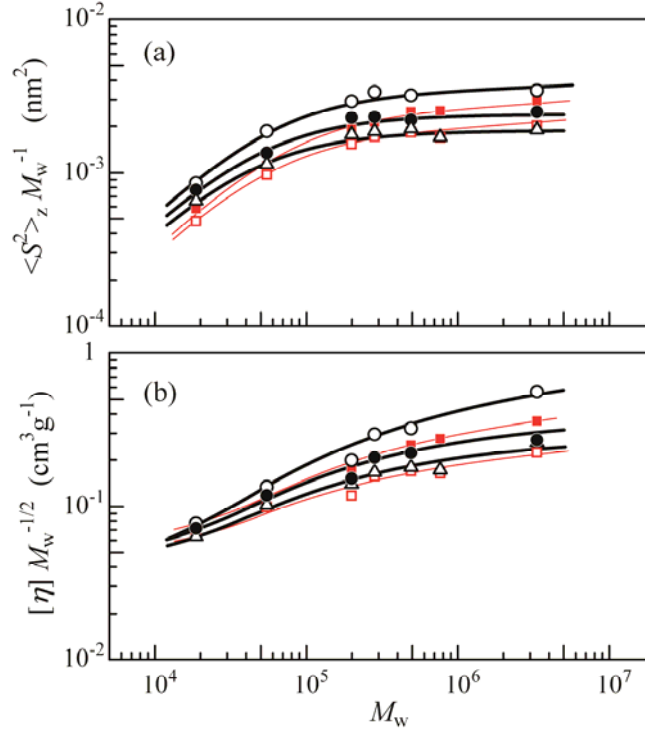
FIGURE 5 Molecular weight dependence of (a) $<S^2>_z M_w^{-1}$ and (b) $[\eta]M_w^{-1/2}$ for ATPC in MEA at 25 °C (triangles), in EA at 33 °C (filled circles), and in MIBK at 25 °C (unfilled circles), compared with previous data[9] in DIOX at 25 °C (filled squares) and in 2EE at 25 °C (unfilled squares).

DISCUSSION

Data analysis in terms of the wormlike chain model – Radius of Gyration

We analyze the present $<S^2>_z$ data in MEA, EA, and MIBK in terms of the wormlike chain whose unperturbed mean-square radius of gyration $<S^2>_0$ is given by[19]

$$\left\langle S^2 \right\rangle_0 = \frac{L}{6\lambda} - \frac{1}{4\lambda^2} + \frac{1}{4\lambda^3 L} - \frac{1}{8\lambda^4 L^2}\left[1 - \exp(-2\lambda L)\right] \tag{1}$$

Here, L is the contour length related to the molar mass M of the chain by

$$L = M/M_L \tag{2}$$

with M_L the molar mass per unit contour length. The two parameters, M_L and λ^{-1}, were determined by curve fitting, but for MIBK solutions, correction was made for excluded-volume effect using the Domb-Barrett equation[20] for the radius expansion factor α_s in the Yamakawa-Stockmayer-Shimada scheme, i.e., the quasi-two-parameter (QTP) theory, [11,21,22] in

which α_s is a universal function of the scaled excluded-volume parameter determined by L, λ^{-1}, and the excluded-volume strength B.

The estimated wormlike-chain parameters in the three solvents are summarized in Table 2, and the theoretical solid lines are compared with the experimental data in Figure 6, in which the dashed line drawn for MIBK refers to the unperturbed state. The fits of the solid curves are satisfactory. It should be noted that the excluded-volume effects on $<S^2>_z^{1/2}$ in MIBK are quite small (less than 4 %) even for the highest M_w sample studied.

Table 2. Wormlike Chain Parameters for ATPC

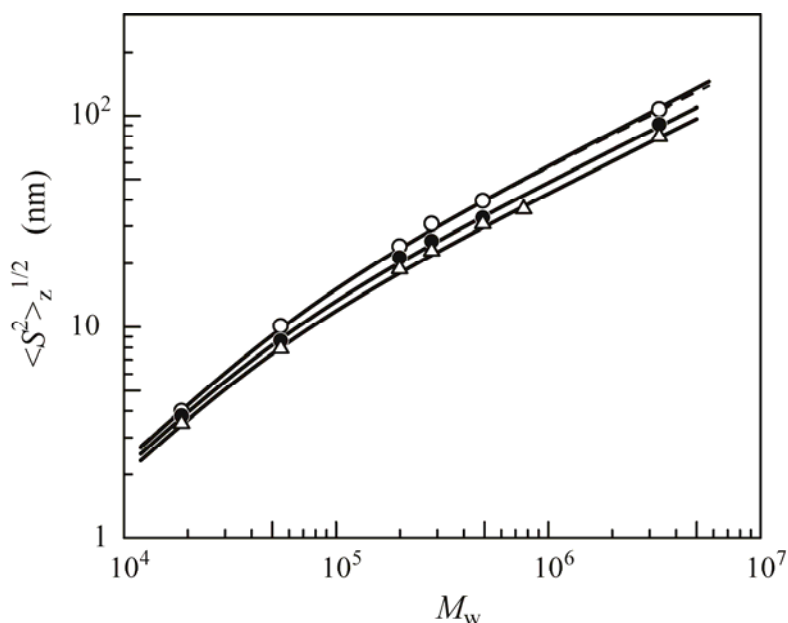| ATPC in MEA at 25 °C				
Method	M_L (nm^{-1})	λ^{-1} (nm)	d (nm)	
$<S^2>_z$	1330 ± 50	15 ± 2	–	
$P(k)$	1390 ± 20	14 ± 2	1.5 ± 0.1	
$[\eta]$	1460 ± 50	14.5 [a]	2.3 ± 0.2	
ATPC in EA at 33 °C				
Method	M_L (nm^{-1})	λ^{-1} (nm)	d (nm)	
$<S^2>_z$	1250 ± 50	18 ± 2	–	
$P(k)$	1310 ± 20	16 ± 2	1.6 ± 0.1	
$[\eta]$	1410 ± 50	17 [a]	2.3 ± 0.2	
ATPC in MIBK at 25 °C				
Method	M_L (nm^{-1})	λ^{-1} (nm)	d (nm)	B (nm)
$<S^2>_z$	1190 ± 50	24 ± 2	–	0.5 ± 0.5
$P(k)$	1230 ± 40	23 ± 3	1.7 ± 0.1	–
$[\eta]$	1310 ± 50	23.5 [a]	1.9 ± 0.2	0.5 [a]

[a] Assumed.

FIGURE 6 Comparison of the experimental $\langle S^2 \rangle_z$ for ATPC in MEA at 25 °C (triangles), in EA at 33 °C (filled circles), and in MIBK at 25 °C (unfilled circles) with the theoretical values calculated for the wormlike chains with the parameters in Table 2. For MIBK solutions, excluded-volume effects are corrected in the QTP scheme[11,21,22] with the Domb-Barrett equation[20] for the radius expansion factor. The dashed curve shows the unperturbed values for $B = 0$.

Particle Scattering Function

Figure 7 shows that the Holtzer plots of $kP(k)$ vs k for low-molar mass samples ATPC20K and ATPC50K in the three solvents have features typical of the wormlike chain with finite thickness. The solid curve fitted to the data points in each panel indeed represents Nakamura and Norisuye's theory[23] for wormlike cylinders. In the curve fitting procedure, the λ^{-1} values for ATPC20K in the three solvents were assumed to be the same as those for ATPC50K in the corresponding solvents. This is because for ATPC20K the dashed lines representing the rod-limiting values ($\lambda^{-1} = \infty$) for the same L and d do not differ much from the solid curves for the wormlike chains with finite λ^{-1}, while those for ATPC50K differ from the solid curves for ATPC50K in the low-k region, allowing unequivocal determination of λ^{-1}.
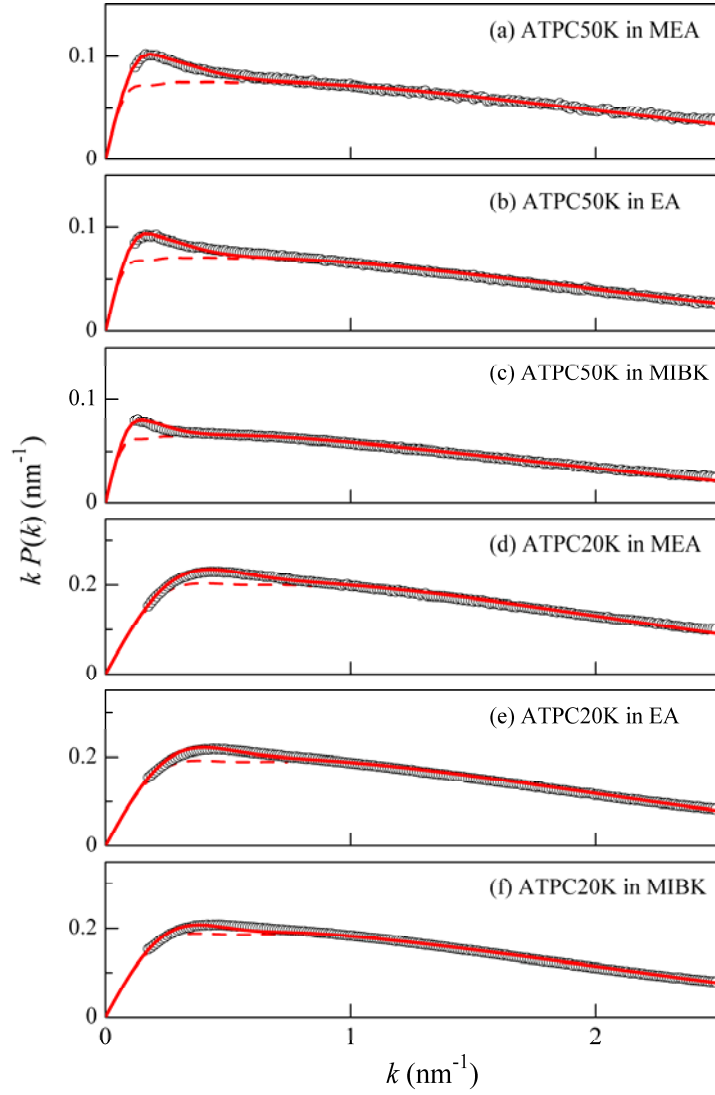
FIGURE 7 Holtzer plots for (a) ATPC50K in MEA at 25 °C; (b) ATPC50K in EA at 33 °C; (c) ATPC50K in MIBK at 25 °C; (d) ATPC20K in MEA at 25 °C; (e) ATPC20K in EA at 33 °C; (f) ATPC20K in MIBK at 25 °C.   Solid curves, theoretical values for the unperturbed wormlike cylinders with the parameters listed in Table 2.   Dashed curves, theoretical values in the rod limit $(\lambda^{-1} = \infty)$.

The values of M_L, λ^{-1}, and d (the chain diameter) thus estimated from $P(k)$ are summarized in Table 2, where for M_L and d, the averages for the two samples in each solvent are given because the difference in either parameter between the two samples is small.   It can be seen that M_L and λ^{-1} from $P(k)$ in the three solvents agree substantially with those from $<S^2>_z$.   Importantly, the mean (1210 nm^{-1}) of the M_L values from these properties in MIBK is slightly smaller than those in the other two solvents and much smaller than the previously estimated value 1540 nm^{-1} in DIOX. This difference in M_L between MIBK and DIOX seems to be more than the uncertainty in our estimation and can indeed be seen directly from that in the height of $kP(k)$ (the so-called Holtzer plateau) around $k = 0.5 - 1$ nm^{-1} for ATPC50K (compare the scattering curve in panel (c) of Figure 7

with that in panel (a) of Figure 8 in ref. 9). Another point to note here is that, when the d values (1.5 – 1.7 nm) in the table are used, the contribution ($d^2/8$) from the chain thickness to $<S^2>_0$ of the cylindrical wormlike chain[24] is found to be about 2 % and hence negligible.

Intrinsic Viscosity

The Yamakawa-Fujii-Yoshizaki theory[11,25,26] for the intrinsic viscosity $[\eta]_0$ of an unperturbed wormlike cylinder contains M_L, λ^{-1}, and d as the parameters. Since all of these three cannot uniquely be determined from the present $[\eta]$ data, we used the mean of λ^{-1} obtained from $<S^2>_z$ and $P(k)$ in each solvent. Excluded-volume effects in MIBK solutions were taken into account by use of the QTP theory with the Barrett equation[27] for the viscosity expansion factor. The estimated parameters are presented in Table 2 and the theoretical $[\eta]$ values are shown by solid curves in Figure 8, in which the dashed line represents the theoretical $[\eta]_0$ in MIBK. The excluded-volume effect is seen to be insignificant even for the highest M_w sample (less than 7%) as is the case with $<S^2>_z$.
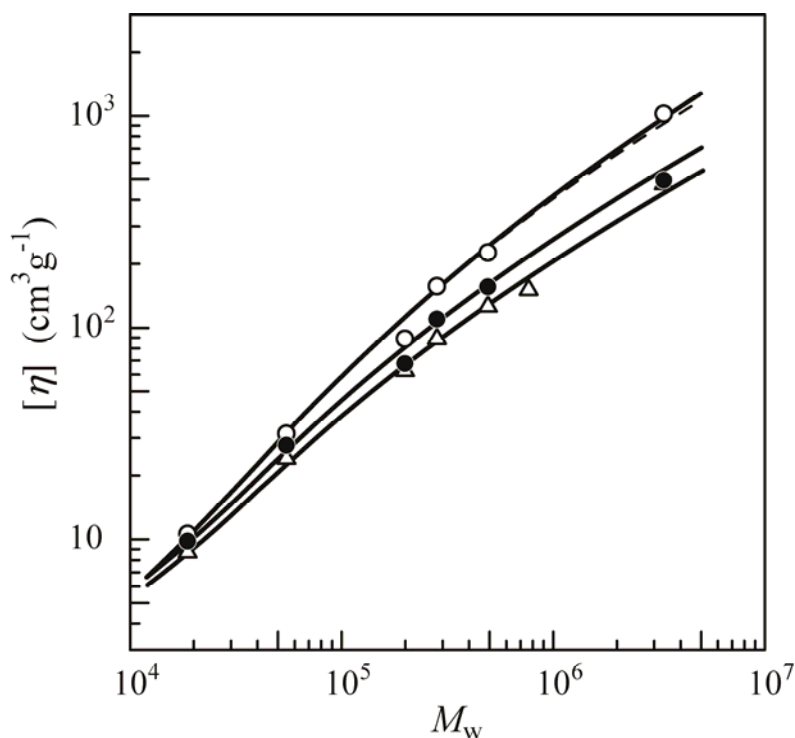

FIGURE 8 Comparison of the experimental $[\eta]$ for ATPC in MEA at 25 °C (triangles), in EA at 33 °C (filled circles), and in MIBK at 25 °C (unfilled circles) with the theoretical values calculated for the unperturbed wormlike cylinders[11,25,26] and the Barrett equation[27] for the viscosity expansion factor in the QTP scheme[11,21,22] with the parameters in Table 2. The dashed curve shows the theoretical values for $B = 0$.

The values of M_L and λ^{-1} determined from $<S^2>_z$, $P(k)$, and $[\eta]$ in the respective solvents essentially agree with one another, leading to the conclusion that the available theories[19,23,25,26] for

the wormlike chain consistently explain the dilute-solution behavior of ATPC. It should be noted that the slightly smaller M_L values from $<S^2>_z$ than those from $P(k)$ and $[\eta]$ in the corresponding solvent are most likely due to the molecular weight distribution of our ATPC samples: The error is estimated to be at most 10% from the value of M_z/M_w (~ 1.1).[9] Although the d values from $P(k)$ and $[\eta]$ do not always agree, the discrepancy may arise from the fact that d from the former can be affected by the electron density profile around the chain contour.[11,28,29] In the ensuing discussion, we use d from $[\eta]$.

Molecular Characteristics in Various Solvents

Table 3 summarizes the means for λ^{-1} and h (= M_0/M_L) and the d values (from $[\eta]$) for ATPC in MEA, EA, and MIBK along with the previously determined values in DIOX and 2EE, where M_0 denotes the molar mass per repeating unit. Interestingly, h varies with the kind of solvent and its difference between MIBK and 2EE amounts to 30%. Furthermore, the values (0.37 – 0.42 nm) in MEA, EA, and MIBK are comparable to the helix pitches (0.37 – 0.40 nm) per residue of amylose triesters in the crystalline state.[14,15] Thus, we may conclude that the shorter helix pitch of about 0.33 nm in DIOX or 2EE mentioned in the Introduction is not specific to ATPC in solution. In other words, the longer pitches or contour lengths per residue in the three polar solvents, the esters and the ketone, may be interpreted as the result of chain extension (along the helix axis) due to the breaking of intramolecular hydrogen bonds between the C=O and NH groups of the polymer; according to our previous IR spectra, about 40% of the groups form hydrogen bonds in DIOX or 2EE. It seems reasonable to consider that the C=O groups of the solvent molecules break these hydrogen bonds and form intermolecular hydrogen bonds with NH groups of the polymer to compensate for the enthalpy loss. Moreover, the solubility of ATPC having LCSTs in all of the three solvents lends support to the presence of such intermolecular hydrogen bonds. On the basis of these considerations, we conjecture that each solvent molecule wedges itself into the domain sandwiched between the neighboring phenylcarbamate groups and that a molecule with a larger v_M (MIBK > EA > MEA) occupies a larger domain to contribute toward extending the helix. This is consistent with the data in Table 3 showing that h is a gradually increasing function of v_M in the three solvents (see Figure 1 for the values of v_M).

   The main-chain stiffness in the three solvents expressed in terms of λ^{-1} also increases slightly with an increase in v_M. We may explain this in a consistent way that the bulkiness of the solvent molecules interacting with the NH groups of ATPC through hydrogen bonding hinders the rotation of each virtual bond and thus stiffens the main chain. As was remarked previously,[9] the ATPC chains in DIOX and 2EE are stiffened by the intramolecular hydrogen bonding between the C=O and NH groups in addition to the bulky-substituent effect intrinsic to ATPC, but we are unable to discuss further the λ^{-1} data in Table 3 in relation to the solvent effect on chain stiffness. In short, the present analysis may be taken to show that, regardless of this effect, the helix pitch per residue gets

longer by 10 – 30% when the intramolecular hydrogen bonds are replaced with the intermolecular ones by exchanging the solvent.

In Table 3, d tends to increase with decreasing h.   This seems reasonable because a more tightly wound helix is generally thicker.   However, the values of d in MIBK, EA, and MEA may be regarded as roughly the same if the uncertainty indicated in Table 2 is taken into consideration. Thus it is only certain that the helices in these solvents are thinner than that with the shorter pitch of 0.33 nm in DIOX or 2EE.   Since, irrespective of the magnitude of v_M, the solvent molecules strongly interacting with the NH groups of ATPC are likely to be embedded in the domains surrounded by the neighboring phenylcarbamate groups, they may hardly contribute to the hydrodynamic diameter.

Table 3.   Values of h, λ^{-1}, and d for ATPC in Various Solvents

Solvent	T (°C)	h (nm)	λ^{-1} (nm)	d (nm) [b]
MIBK	25	0.42 ± 0.02	24 ± 2	1.9
EA	33	0.39 ± 0.02	17 ± 2	2.3
MEA	25	0.37 ± 0.02	15 ± 2	2.3
DIOX [a]	25	0.34 ± 0.01	22 ± 2	2.9
2EE [a]	25	0.32 ± 0.01	16 ± 2	2.8

[a] Ref 9. [b] From $[\eta]$.

CONCLUSIONS

Light and small-angle X-ray scattering and viscosity data for ATPC samples in MEA at 25 °C, in EA at 33 °C, and in MIBK at 25 °C, all of which are capable of strongly interacting with the NH groups of the polymer, are presented and analyzed on the basis of the wormlike chain.   The following conclusions may be drawn from the analysis.

1. MEA at 25 °C and EA at 33 °C are theta solvents for the amylose derivative whose Kuhn segment lengths are as large as 15 – 24 nm; the theta state has seldom been found for linear polymers with such high stiffness.[30]

2. The estimated h values (0.37 – 0.42 nm) in MEA, EA, and MIBK are comparable to the helix pitches (0.37 – 0.40 nm) per residue of amylose triesters in the crystalline state, so that the previously found shorter helix pitch of about 0.33 nm in DIOX or 2EE is not specific to ATPC in solution.

3. Both h and λ^{-1} in the esters and the ketone slightly increase with increasing solvent molar volume, indicating that the bulkiness of the polar solvent molecules tends to extend the helix and to stiffen the main chain.

REFERENCES
1. Burchard, W. Z Physik Chem 1964, 42, 293-313.
2. Burchard, W. Makromol Chem 1965, 88, 11-28.
3. Banks, W.; Greenwood, C. T.; Sloss, J. Eur Polym J 1971, 7, 879-888.
4. Burchard, W. Br Polym J 1971, 3, 214-221.
5. Sutter, W.; Burchard W. Makromol Chem 1978, 8, 1961-1980.
6. Pfannemüller, B.; Schmidt, M.; Ziegast, G.; Matsuo, K. Macromolecules 1984, 17, 710-716.
7. Muroga, Y.; Hayashi, K.; Fukunaga, M.; Kato, T.; Shimizu, S.; Kurita, K. Biophys Chem 2006, 121, 96-104.
8. Bittiger, H.; Keilich, G. Biopolymers 1969, 7, 539-556.
9. Terao, K.; Fujii, T.; Tsuda, M.; Kitamura, S.; Norisuye, T. Polym J 2009, 41, 201-207.
10. Kratky, O.; Porod, G. Recl Trav Chim Pays-Bas 1949, 68, 1106-1122.
11. Yamakawa, H. Helical Wormlike Chains in Polymer Solutions; Springer: Berlin, 1997.
12. Nakanishi, Y.; Norisuye, T.; Teramoto, A.; Kitamura, S. Macromolecules 1993, 26, 4220-4225.
13. Norisuye, T. Polym J 1994, 26, 1303-1307.
14. Zugenmaier, P.; Steinmeier, H. Polymer 1986, 27, 1601-1608.
15. Takahashi, Y.; Nishikawa, S. Macromolecules 2003, 36, 8656-8661.
16. Kasabo, F.; Kanematsu, T.; Nakagawa, T.; Sato, T.; Teramoto, A. Macromolecules 2000, 33, 2748-2756.
17. Kitamura, S.; Yunokawa, H.; Mitsuie, S.; Kuge, T. Polym J 1982, 14, 93-99.
18. Berry, G. C. J Chem Phys 1966, 44, 4550-4564.
19. Benoit, H.; Doty, P. J Phys Chem 1953, 57, 958-963.
20. Domb, C.; Barrett, A. J. Polymer 1976, 17, 179-184.
21. Yamakawa, H.; Stockmayer, W. H. J Chem Phys 1972, 57, 2843-2854.
22. Shimada, J.; Yamakawa, H. J Chem Phys 1986, 85, 591-599.
23. Nakamura, Y.; Norisuye, T. J Polym Sci Part B: Polym Phys 2004, 42, 1398-1407.
24. Konishi, T.; Yoshizaki, T.; Saito, T.; Einaga, Y.; Yamakawa, H. Macromolecules 1990, 23, 290-297.
25. Yamakawa, H.; Fujii, M. Macromolecules 1974, 7, 128-135.
26. Yamakawa, H.; Yoshizaki, T. Macromolecules 1980, 13, 633-643.
27. Barrett, A. J. Macromolecules 1984, 17, 1566-1572.
28. Hickl, P.; Ballauff, M.; Scherf, U.; Mullen, K.; Lindner, P. Macromolecules 1997, 30, 273-279.
29. Terao, K.; Mizuno, K.; Murashima, M.; Kita, Y.; Hongo, C.; Okuyama, K.; Norisuye, T.; Bächinger, H. P. Macromolecules 2008, 41, 7203-7210.
30 Norisuye, T. Prog Polym Sci, 1993, 18, 543-584.